Two-dimensional salt and temperature DNA denaturation analysis using a magnetoresistive sensor

Rizzi, Giovanni; Dufva, Martin; Hansen, Mikkel Fougt

Published in:
Lab on a Chip

Link to article, DOI:
10.1039/c7lc00485k

Publication date:
2017

Document Version
Peer reviewed version

Two-dimensional salt and temperature DNA denaturation analysis on a magnetoresistive sensor

Giovanni Rizzi,[a] Martin Dufva[a] and Mikkel Fougt Hansen[a†]

We present a microfluidic system and its use to measure DNA denaturation curves by varying temperature or salt (Na^+) concentration. The readout is based on real-time measurements of DNA hybridization using magnetoresistive sensors and magnetic nanoparticles (MNPs) as labels. We report the first melting curves of DNA hybrids measured as function of continuously decreasing salt concentration at fixed temperature and compare to corresponding curves obtained vs. temperature at fixed salt concentration. The magnetoresistive sensor platform provided reliable results under varying temperature as well as salt concentration. The salt concentration melting curves were found more reliable than temperature melting curves. We performed a two-dimensional mapping of the melting profiles of a target to probes targeting its wild type (WT) and mutant type (MT) variants in the temperature-salt concentration plane. This map clearly showed a region of optimum ability to differentiate between the two variants. We finally demonstrated single nucleotide polymorphysm (SNP) genotyping using both denaturation methods both on separate sensors but also using a differential measurement on a single sensor. The results demonstrate that concentration melting provides an attractive alternative to temperature melting in on-chip DNA denaturation experiments and further show that the magnetoresistive platform is attractive due to its low cross-sensitivity to temperature and liquid composition.

1. Introduction

The detection of DNA mutations is most often carried out using allele specific probes that have sequence complementary to the wild type (WT) and mutant type (MT) variants of the investigated gene. Target DNA binds to the probes through hydrogen bonds between complementary bases in the probe and the target sequences. The sugar-phosphate backbone that forms the framework of each strand is negatively charged and this charge would separate the two DNA strands if not shielded by positive ions in solution. Therefore, the stability of the double stranded DNA helix depends on the cation concentration as well as on the temperature of the solution. The temperature and salt concentration are experimental parameters that can be often controlled and are generally termed stringency. By increasing stringency (higher temperature or lower salt concentration) it is possible to cause denaturation of the double stranded DNA.[1]

The specificity of DNA hybridization can be used for genotyping via a number of different assay strategies and is now routinely used in analysis laboratories. Due to the potential application in point of care diagnostics, many of these have been implemented on lab-on-a-chip platforms for genotyping.[2]

Hybridization to surface immobilized DNA probes is particularly attractive because it offers possibility for multiplexed investigation of multiple sites. This forms, for example, the basis for DNA microarrays where the target interaction with up to thousands of probes is investigated simultaneously. In these, the difference in fluorescence signal between spots of WT and MT probes is determined at end-point after introduction of a fluorophore-labeled target and a stringent wash. Under low-stringency conditions (low temperature and high salt concentration) the hybridization is tolerant to mismatches and the target binds to both WT and MT probes, whereas at high-stringency conditions (high temperature and low salt concentration) the target will only bind to the perfectly matching probe.

The optimization of probe lengths and conditions during the stringent wash to facilitate discrimination between WT and MT variants while still maintaining a clear signal from the matching target is a design challenge that increases tremendously with the number of targets.[3,4]

It is therefore attractive to detect the signal during a continuous increase of stringency such that discrimination can be made at optimum stringency conditions for each of the probes investigated. It is possible to determine the temperature and salt concentration condition that causes DNA hybrids to denature by continuously increasing temperature or decreasing ionic concentration (Figure 1b). In the literature, measurements of the melting of DNA hybrids have been performed as function of increasing temperature using readouts based on fluorescence[5–7], electrochemistry[8–10], surface plasmon resonance (SPR)[11,12], surface enhanced Raman spectroscopy (SERS)[13], and magnetoresistive sensors[14]. Several of these readouts have significant cross-sensitivities to temperature and salt concentration and thus require extra care. Further, only very few studies have varied stringency using a ramping of the salt concentration.[15]

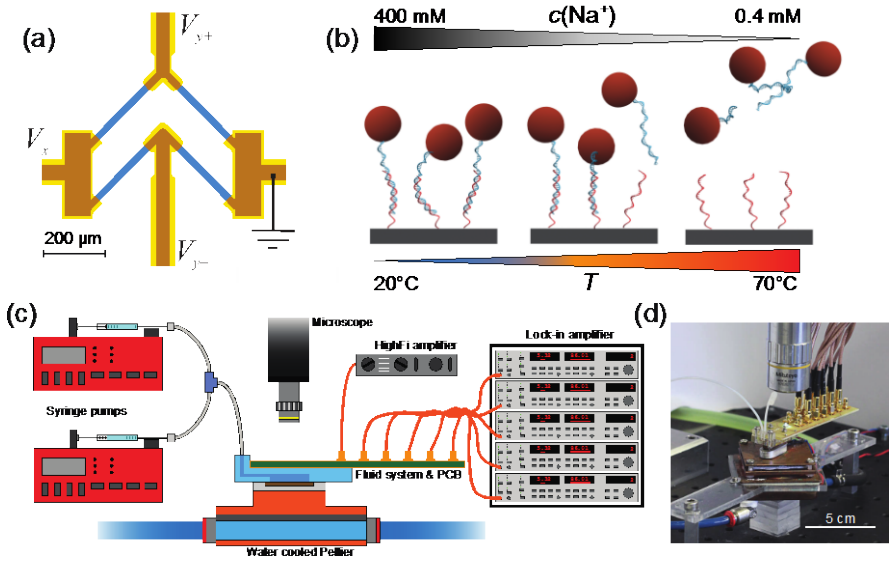

Figure 1: (a) Schematics of the differential magnetoresistive sensor bridge. The magnetic material is shown in blue, electrical contacts in yellow. V_x is the sensor bias voltage and V_y is the sensor bridge output voltage. **(b)** Schematic of temperature and salt concentration melting. Increasing temperature or decreasing salt concentration increases the stringency causing denaturation of the target-probe hybrids. Following denaturation, MNP-labeled targets are released from the sensor surface resulting in a reduced signal from the sensor bridge. **(c)** Schematic of the measurement setup. **(d)** Chip holder setup. The chip is mounted in the microfluidic chamber below the circuit board that provides electrical connection to the chip via spring-loaded pins.

Magnetoresistive sensors have been employed in lab-on-a-chip systems for the detection of DNA as well as proteins. In the most common assay format, the sensors detect binding of the target labelled with magnetic tags to the sensor surface, functionalized to specifically capture the target (using, e.g., DNA probes or antibodies).[16,17] Detecting magnetic nanoparticle labels present an attractive approach as magnetic sensors are only very weakly sensitive to variations in temperature and salt concentration.[14,18,19] Further, they can be made in a compact format and with a scalable number of sensors.[20]

Recently, we demonstrated the use of so-called planar Hall effect bridge (PHEB) sensors for real-time measurements of the temperature melting of DNA hybrids.[14] In the present work, we further investigate the combined effect of temperature and salt concentration. We demonstrate two-dimensional salt and temperature denaturing mapping of a target to WT and MT probes to investigate salt concentration melting and to identify optimum conditions for discrimination between matching and mismatching target-probe hybrids. We further investigate the use of a single sensor bridge to discriminate between WT, MT and a mixture of these targets.

2. Material and methods

2.1 Sensor fabrication

The magnetoresistive sensor bridges were fabricated as described previously.[19] Briefly, anisotropic magnetoresistive elements of nominal composition Ta(5 nm)/$Ni_{80}Fe_{20}$(30 nm)/ $Mn_{80}Ir_{20}$(10 nm)/ Ta(5 nm) were sputter-deposited in a saturating magnetic field. Electrical contacts of Ti(10 nm)/ Pt(100 nm)/Au(100 nm)/Ti(10 nm) were deposited by electron beam evaporation. The sensors were spin coated with a 900 nm thick passivation layer (Ormocomp, Micro Resist Technology, GmbH, Germany).

A chip comprised five differential magnetoresistive sensor bridges – each consisting of four sensor elements with length l=250 µm and width w=25 µm (Fig. 1a). This sensor design (termed differential planar Hall effect bridge, dPHEB) measures the differential signal between the top two branches and the bottom two branches of the bridge as described by Rizzi *et al.*[19]

2.2 Measurement platform

The measurement platform was previously described by Østerberg *et al.*[21] and Rizzi *et al.*[19] and is depicted in Fig. 1c. The chip was mounted in a click-on microfluidic system defining a fluidic channel (width × height × length= 1 mm × 1 mm × 5 mm) over the sensor surface and providing electrical contact to the magnetoresistive sensors using spring-loaded pins (Fig. 1d).

A sinusoidal voltage of V_{RMS}=1.6 V at frequency f=167 Hz was applied to all sensor bridges connected in parallel using a commercial audio amplifier. The output voltage of each sensor bridge was measured using an SR830 Lock-In amplifier with an SR552 preamplifier (Stanford Research Systems, Inc., USA). The MNPs were magnetized by the magnetic field due to the applied bias current through the sensor and the presence of MNPs on the sensor was detected in the imaginary part of the second harmonic lock-in signal.[19]

The sensor chip was mounted in an aluminum chip holder with good thermal contact. The temperature of the chip mount was measured with a Pt1000 thermometer, and controlled via a LFI3751 control unit (Wavelength Electronics, USA) driving a Peltier element. The other side of the Peltier

element was cooled using a commercial CPU water cooling system.

Two syringe pumps (model 540060, TSE systems, Germany), connected to a chip inlet via a T-branch, provided the liquid flow in the chip during washing. They were controlled via a custom LabView program such that any ratio of the two liquids could be injected while maintaining a constant total liquid flow rate.

2.3 Experimental procedure

2.3.1 Sensor functionalization

The sensor elements on each of the five sensor bridges could be selectively functionalized with amino modified ssDNA probes as described by Rizzi *et al.*[19] The probes to genotype SNPs in the *human beta globin* (*HBB*) gene (sequences in Supplementary Information) were adapted from Petersen *et al.*[7] and were purchased from DNA Technology A/S, Denmark.

One of the sensor bridges on each chip was used as a positive reference and was functionalized on its top half with a biotinylated DNA probe.

Two sensor bridges were used for direct detection of the wild type (WT) or mutant type (MT) variants of the CD 8/9 locus of the *HBB* gene and were functionalized on their top halves with the corresponding respective probes. We will refer to these as the MT and WT sensors, respectively.

To perform WT-MT differential detection of the CD 8/9 and CD 17 loci of the *HBB* gene, two sensor bridges on a chip were functionalized on their top and bottom halves with probes matching the WT and MT variants, respectively.

2.3.1 Hybridization

The solution of target-labeled MNPs was prepared by mixing a solution of 10 nM biotinylated target DNA (sequences in supplementary information) in 4×Saline Sodium Citrate (SSC, Gibco, USA) buffer 1:1 v:v with the stock solution of Miltenyi Streptavidin Microbeads (Miltenyi Biotec Norden AM, Sweden) to a final target concentration of 5 nM (buffer salt concentration $c(Na^+)$=400 mM).

The streptavidin coated particles have a nominal diameter of 50 nm and each multicore particle contains about twelve γ-Fe_2O_3 magnetic cores with a diameter of about 13 nm.[22] The target-MNP solution was injected over the sensors and incubated for 30 min at T=37°C.

2.3.2 Temperature melting

After hybridization of WT DNA target, the chip was washed with diluted SSC buffer to a final concentration $c(Na^+)$=10 mM or 2 mM at T=20°C for 80 s at 30 μL/min. Following washing, the temperature was ramped from T=20°C to 70°C at 0.1°C/s. The melting data was corrected for the temperature dependence of the sensor sensitivity using a reference sweep from T=70°C to 20°C measured after complete denaturation of the hybrids as described previously.[14]

2.3.3 Salt concentration melting

After hybridization of WT DNA target, the chip was washed with 2×SSC ($c(Na^+)$=400 mM) at T=30°C or 40°C at 30 μL/min for 80 s. After this initial washing, the washing buffer concentration was varied exponentially from $c(Na^+)$=400 mM to 0.4 mM over 1200 s by mixing the flow of 2×SSC buffer from syringe pump one with milliQ water from syringe pump two. Concentration dependent sensor offsets determined from a reference concentration profile measurement with no MNPs were subtracted from the data.

2.3.4 WT-MT differential measurements

Three 5 nM target DNA solutions were analyzed on the sensor bridges functionalized for WT-MT differential detection: WT, MT and 1:1 WT:MT. After hybridization, melting curves were measured during both temperature and salt concentration melting. Temperature melting was performed as described above with $c(Na^+)$=10 mM. Salt concentration melting was performed as described above at T=37°C. The signal measured during temperature melting was corrected for the temperature dependence of the sensor sensitivity and normalized by the signal from the positive reference sensor functionalized with biotinylated DNA.

3. Results

3. 1 Temperature melting

Biotinylated WT DNA target, labeled with streptavidin MNPs, at a DNA concentration of c=5 nM in 2×SSC buffer ($c(Na^+)$=400 mM) was incubated over the sensors at T=37°C for 30 min. The measurements below were performed with the WT and MT sensors for SNP detection of the CD 8/9 locus in *HBB* (see inset in Fig. 2b). The signal due to MNPs was measured in the imaginary part of the 2nd harmonic bridge voltage, here written as V, in response to the AC bias of the bridge.[19] When the top and bottom halves of the bridge experience the same concentration and distribution of MNPs, the bridge is balanced and nominally zero signal is detected. Hybridization of MNP-labeled DNA to the top half of a sensor bridge increases the local MNP concentration at this half of the sensor bridge and causes an increase of V.[19]

After hybridization, the chip temperature was decreased to T=20°C to stabilize hybrids and inhibit further binding. Unbound target-MNPs were removed by washing. Two buffers were tested, with $c(Na^+)$=10 mM and 2 mM, respectively. Following washing, the buffer was left stagnant over the sensors and the temperature was ramped from T=20°C to 70°C at 0.1°C/s to measure the melting of the DNA hybrids in real time.

Figure 2 shows the WT target melting curves measured for $c(Na^+)$=10 mM and 2 mM, respectively. The real-time data was corrected for the temperature dependence of the sensor output and normalized to the initial value at 20°C.

For $c(Na^+)$=10 mM (Fig. 2a) the signals for both the WT and MT sensors were stable between 20°C and 30°C. At T > 30°C, the signal from the MT sensor decreased sharply indicating a temperature melting of the DNA hybrids. For the WT sensor,

the melting was shifted to a higher temperature. Some variation in the absolute melting temperatures was observed between the three experiments. However, in each experiment, we found the temperature shift between the MT and WT sensors to be reproducible and with a value of about 8°C.

For $c(Na^+)$=2 mM (Fig. 2b) the results followed a similar trend. The MT sensor signal showed a sharp decrease at a temperature, which was about 9°C lower than for the WT signal. Compared to Fig. 2a, the melting also took place at lower temperature.

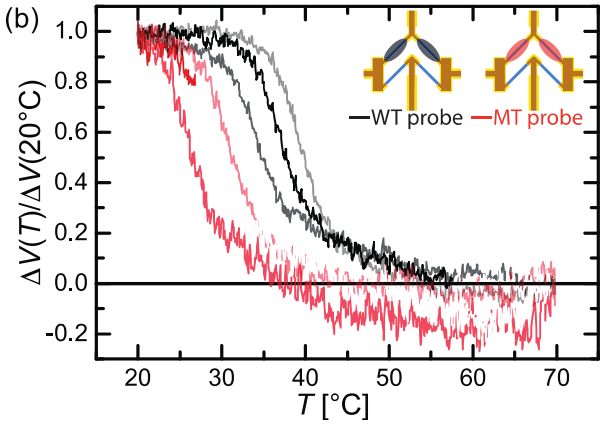

Figure 2: Temperature melting curves of MNP labeled WT DNA target hybridized to WT (black) and MT (red) DNA probes for the CD8/9 mutation. The two sensor bridges were functionalized as depicted in the inset. The DNA hybrids were denatured by increasing the temperature from T=20°C to 70°C at 0.1°C/s for **(a)** $c(Na^+)$=10 mM and **(b)** $c(Na^+)$=2 mM. Results of triplicate experiments are shown.

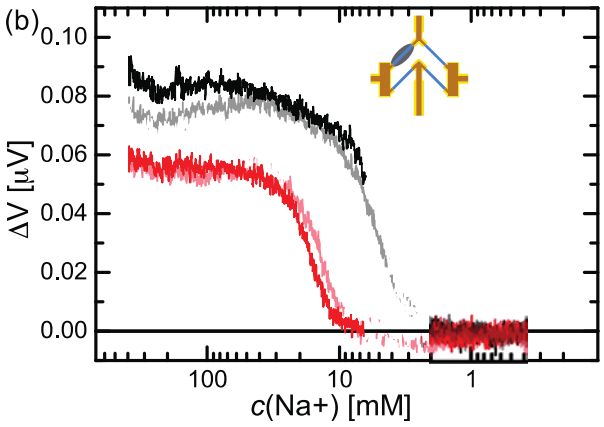

Figure 3: Salt concentration melting curves of WT DNA target hybridized to WT (black) and MT (red) DNA probes for the CD8/9 mutation. PHEB sensors were functionalized as depicted in the inset. The hybrids were denatured by decreasing the salt concentration from $c(Na^+)$=400 mM to 0.4 mM over 1200 s at **(a)** T=30°C and **(b)** T=40°C. Results of triplicate experiments are shown.

3.2 Salt concentration melting

Melting measurements of the MNP-labeled WT DNA hybrids were also performed at fixed temperature as function of decreasing salt concentration in the washing buffer. Following hybridization, the sensor temperature was set to 30°C or 40°C and unbound labels were washed off with 2×SSC buffer ($c(Na^+)$=400 mM) at a flow rate of 30 µL/min. Subsequently, the washing buffer salt concentration was exponentially decreased from $c(Na^+)$=400 mM to 0.4 mM over 1200 s while maintaining a constant total flow rate of 30 µL/min by varying the relative flow rate of the two syringe pumps loaded with 2×SSC and MilliQ water, respectively. Salt concentration melting curves were measured in real-time during the decreasing concentration profile. Figure 3 shows the results obtained at T=30°C and 40°C; a logarithmic time scale is used because of the exponential time profile of the buffer concentration. The final value of the sensor signal at $c(Na^+)$=0.4 mM was subtracted to obtain the signal variation $\Delta V(c)$.

At T=30°C (Fig. 3a), the signals for both WT and MT sensors were approximately constant at high salt concentrations, $c(Na^+)$ > 20 mM, and the WT sensor signal was 25% higher than

that from the MT sensor. The three experiments were highly reproducible and therefore no normalization of the data was performed. The MT sensor signal decreased sharply between $c(Na^+)$=20 mM and 2 mM indicating a melting of the DNA hybrids. The signal from WT probe decreased at a lower salt concentration $c(Na^+)$ < 3 mM.

At T=40°C (Fig. 3b), the same trend was observed, but the melting curves were shifted to higher salt concentrations, such that melting took place at higher $c(Na^+)$ compared to T=30°C.

3.3 Melting temperature T_m and concentration c_m

Error function fits to the temperature melting curves in Fig. 2 were performed to extract the melting temperature T_m defined as the temperature at which the curve reached 50% of its initial value. For $c(Na^+)$=10 mM we obtained T_m(WT)=43±1°C and T_m(MT)=35±1°C (uncertainties indicate standard error of the mean (SDOM), n=3) for the WT and MT sensors, respectively. The corresponding values for $c(Na^+)$=2 mM were T_m(WT)=38±1°C T_m(MT)=29±1°C.

Similarly, error function fits to the data in Fig. 3 vs. log(c) were performed to extract the melting concentration c_m, defined as the point at which the error function reached 50% of the initial value. At T=30°C we obtained c_m(WT)=1.4±0.1 mM and c_m(MT)=6.3±0.3 mM and at T=40°C we obtained c_m(WT)=5.7±0.2 mM and c_m(MT)=15±1 mM. Uncertainties indicate SDOM (n=3).

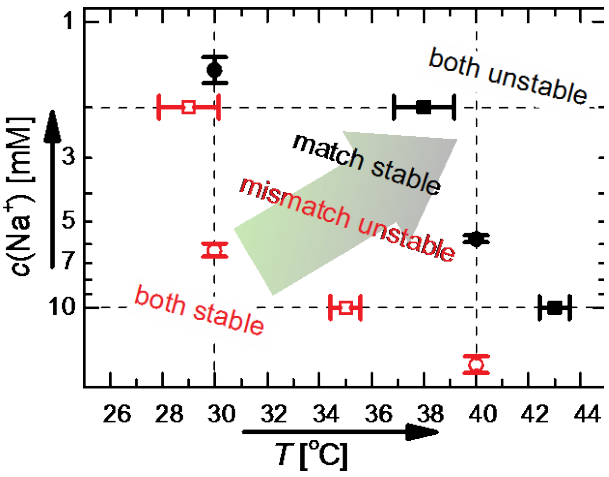

Figure 4: Values of melting temperature T_m and salt concentration c_m obtained from error function fits to the temperature and salt melting, respectively, for the WT target and WT probes (filled black symbols) and MT probes (open red symbols) for the CD 8/9 locus of *HBB*. Dashed lines represent the temperature (horizontal) and concentration (vertical) profiles used. The arrow indicates direction of increasing stringency. Error bars are standard error of the mean (n=3).

The values of T_m and c_m obtained from the denaturation experiments are collected in Fig. 4. The dashed lines represent the temperature or concentration profiles used. The perfectly matched WT probe-WT target gave denaturation points at higher stringency compared to the mismatched MT probe-WT target hybrids. The separation between the two is not constant, but it is maximal in the central region of the plot.

3.4 Genotyping using WT-MT differential measurements

We have previously shown that a single sensor bridge can be used for genotyping when its top and bottom halves are functionalized with WT and MT probes, respectively.[14] The sensor output is proportional to the difference in the amount of MNPs bound to the top and bottom halves of the sensor bridge. To genotype each of the CD 8/9 and CD 17 loci of the *HBB* gene with respect to the mutations given in Table S1, we functionalized a sensor bridge with WT and MT probes on its top and bottom halves, respectively (see insets in Fig. 5). Three target combinations were measured: WT, MT and 1:1 WT:MT.

Figure 5a shows the temperature melting curve measured at $c(Na^+)$=10 mM for the CD 8/9 locus. Note that the curves show the signal relative to that obtained from the positive reference sensor. At low temperature, the relative signal was close to zero for all three targets, indicating identical hybridization of the targets to both WT and MT probes. At temperatures T=30°C to 50°C, the relative signal from the three target clearly differed from each other. For the WT target, the relative signal peaked at a positive value of 0.17 whereas for the MT target, the signal peaked at a negative value of −0.15. The signal from the 1:1 WT:MT target mixture maintained a value closer to zero and reached a minimum value of −0.06. Above T=50°C the relative signal for the three targets stabilized at zero.

Figure 5b shows the salt concentration melting curve measured at T=37°C for the CD 8/9 locus. At high salt concentration ($c(Na^+)$ > 50 nM) the WT and MT targets showed similar values in the range ΔV=–0.005 µV to 0 µV. The signal from the mixed WT:MT target showed a lower value (ΔV=−0.021µV) that increased towards zero for increasing $c(Na^+)$. For $c(Na^+)$=40 nM to $c(Na^+)$=4 nM, the three targets showed maximum separation, with the WT target reaching ΔV=+0.023 µV, the MT target reaching ΔV=−0.023 µV, and the mixed MT:WT target showing a stable signal near ΔV=0 µV. At low salt concentration ($c(Na^+)$<4nM) the signals from the three targets stabilized at zero.

Figures 5c and 5d show the corresponding temperature and salt concentration melting profiles measured for the CD 17 locus. In the temperature melting study (Fig. 5c), the three targets showed a clear separation even at low temperature. The trend with temperature was the same as for the CD 8/9 locus except that the peaks appeared at lower temperatures and the peak levels were slightly lower. The maximum separation between the three targets was observed between 35°C and 40°C. In the salt concentration melting study (Fig. 5d), the three targets were initially separated at high $c(Na^+)$ with ΔV(WT) > ΔV(WT:MT) > ΔV(MT) > 0. Upon increasing stringency (decreasing $c(Na^+)$), ΔV for all three targets decreased and separated more from each other. The largest separation was observed for $c(Na^+)$=29 mM and corresponded to ΔV(MT)=+0.015 µV, ΔV(MT)=−0.008 µV, and ΔV(WT:MT)= +0.002 µV. For $c(Na^+)$<7 mM, the signal from all targets approached ΔV=0.

4. Discussion

4.1 Melting curves

The differential design of the bridge sensors allowed for real-time measurement of the formation and melting of DNA hybrids. The integration of the sensor chip in a microfluidic system with temperature and salt concentration control allowed us to perform two-dimensional melting studies as function of temperature and/or salt concentration. Both of these two parameters affect the stability of DNA hybrids and can thus be used to discriminate between perfectly matched target-probe hybrids and mismatches down to a single nucleotide level. The magnetic sensor platform is compact and sufficiently robust to enable readout under conditions of varying temperature or salt concentration. Both temperature and salt concentration melting curves were measured to characterize the investigated loci of the *HBB* gene. In both investigations, the unmatched MT probe-WT target duplexes denatured at lower stringency (lower T, higher $c(Na^+)$) compared to the perfectly matched counterparts. As expected from nearest neighbor models, decreasing buffer $c(Na^+)$ leads to lower T_m for both matched and mismatched hybrids. Similarly, increasing T leads to higher c_m.

The two methods showed clear differences in reproducibility. While salt concentration denaturation curves (Fig. 3) were almost perfectly overlapping, the absolute melting temperatures measured for repeated measurements showed an uncertainty of about 2°C (SDOM, n=3). The differences in the simultaneously measured melting temperatures measured for the two sensors, $\Delta T_m = T_m(WT) - T_m(MT)$, were found to ΔT_m=7.7±0.2°C ($c(Na^+)$= 10 mM) and 8.9±0.5°C ($c(Na^+)$=2 mM), where the stated uncertainties are SDOM (n=3). Thus, the uncertainty on ΔT_m was significantly lower than that on the absolute melting temperature. This indicates that it was difficult to accurately replicate identical temperature profiles. The variation in the absolute temperature may, for example, originate from differences in temperature of the washing buffer or the chip surroundings. Our results further indicate that salt concentration profiles are more easily reproduced. Moreover, the signal from the magnetoresistive sensors is only weakly sensitive to a

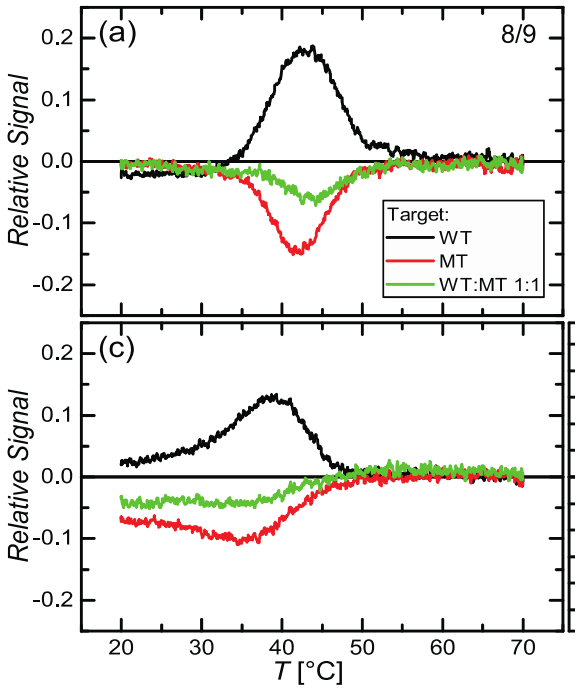

MT probe

Figure 5: Melting curves (**a** and **c**) and salt concentration denaturation curves (**b** and **d**) measured on differential sensors for WT, MT, and a 1:1 WT:MT mixture of target DNA. The sensors were functionalized with WT and MT probes for the CD 8/9 locus (**a** and **b**) or the CD 17 locus (**c** and **d**) as indicated in the insets.

change in the salt concentration. Further, the requirements for temperature control are less restrictive for salt concentration melting and the concentration can be varied using a simple two-pump setup. Therefore, concentration melting experiments are easier to implement.

4.2 Two-dimensional mapping of T_m and c_m

The measurements of the melting curves as function of both temperature and salt concentration allowed us to map the point of denaturation over these two dimensions of experimental conditions. The resulting map of Figure 4 presents the measured T_m and c_m. These results offer a non-trivial insight into the stability of DNA hybrids over a wide range of stringencies in the (T, $c(Na^+)$)-plane.

Hybridization-based assays aim to discriminate between matched and mismatched probe-target hybrids. In an end-point detection scheme, this is done by selecting a stringency condition that, to the extent possible, denatures mismatched hybrids and maintains the matched hybrids. Similarly, a denaturation assay should maximize the gap between the melting points of the matched and mismatched hybrids. In Figure 4 we can identify an optimal region between T=32-38°C and $c(Na^+)$=3-7 mM where the distance between red and black symbols is maximal.

As a perspective, the presented magnetoresistive sensor detection scheme and setup allows for any profile in the (T, $c(Na^+)$)-plane, i.e., for a simultaneous change of T and $c(Na^+)$. Figure 4 indicates that a potentially better separation between WT and MT could be obtained along the diagonal in the (T, $c(Na^+)$)-plane by simultaneously ramping the temperature up and the salt concentration down. This will be topic for future investigation.

Magnetoresistive sensor arrays with up to thousand sensors have been presented in the literature.[20] Real-time two-dimensional maps of the melting of a DNA target hybridized to an array of WT and MT detection probes enable a highly parallel screening of conditions for a range of sequences and probe lengths to target a number of loci and genes in a DNA target. This can be used for direct genotyping but also to identify regions on the (T, $c(Na^+)$)-plane that are optimal for end-point detection after a stringent washing. This could significantly ease the design and improve performance of microarrays, where the probe design may be challenging as a single stringent wash has to produce a large difference between matching and mismatching hybrids while still maintaining a significant signal from the matching hybrids.[7]

4.3 Genotyping using WT-MT differential measurements

By functionalizing the top and bottom halves of a single sensor bridge with WT and MT probes, it was possible to measure the differential binding of target to the two probes. For a given sensor array, this configuration allows for the investigation of a higher number of mutation sites, since only a single sensor is used for each mutation.

The melting curves of Fig. 5 showed different behaviors for the CD 8/9 and CD 17 loci. The stability of the target-probes hybrids depends on the length of the probe, its C+G content and the type of mutation investigated. Here, the mutation at the CD 8/9 locus is a single base (C) insertion, whereas that at the CD 17 locus is a single base (T>A) transversion. The probes had lengths of 22 bases (C+G 54%) and 18 bases (C+G 66%) for the CD 8/9 and CD 17 loci, respectively.

The shorter probe length for CD 17 caused a separation of the three targets also at low stringency (Figs. 5c-d) and maximum separation between the targets was found at lower stringencies compared to CD 8/9. Moreover, the base insertion in CD 8/9 resulted in more unstable mismatched hybrids and caused a higher separation between the three targets (Figs. 5a-b).

For the CD 8/9 locus, the initial negative signal from the 1:1 WT:MT mixed target at high $c(Na^+)$ in Fig. 5b is likely caused by a higher affinity of the MT target-MT probe hybrids compared to that of the WT target-MT probe. This is supported by the observation that the signal from the MT target peaks at lower $c(Na^+)$ (higher stringency) than the WT target in Fig. 5b.

For the salt concentration melting for the CD 17 locus (Fig. 5d), the initial signals from all three targets at high $c(Na^+)$ were positive and were found to decrease with decreasing salt concentration. We speculate that this is caused by higher unspecific binding to the WT probe than the MT probe.

The different behavior of the WT and MT probes for the CD 8/9 and CD 17 loci would require optimization of the assay in end-point detection to determine the optimum washing stringency to perform a correct genotyping. Instead, using a denaturation curve method, the hybrids are subject to a continuously varying stringency and thus we could easily differentiate the three different target compositions.

5. Conclusions

We demonstrated the use of a magnetoresistive sensor array integrated in a lab-on-a-chip system for studies of the denaturation of DNA hybrids as function of both temperature and salt concentration. The magnetic readout was only weakly sensitive to the varying experimental conditions and could therefore be used to provide a sensitive real-time readout of the signal from the magnetic nanoparticle labeled DNA target hybridized to detection probes. The differential sensor design enabled studies of the specific binding of a WT target to WT and MT detection probes for two loci of the human *HBB* gene. Melting experiments at different cuts in the temperature-salt concentration plane identified a region of optimal discrimination between the two. Further, it was found that salt concentration melting curves were more reproducible than temperature melting curves. These provide a hitherto not studied but interesting alternative to temperature melting curves in lab-on-a-chip systems.

Further, we demonstrated the discrimination between WT, MT and 1:1 WT:MT targets using a single sensor bridge functionalized on its top and bottom parts with WT and MT probes, respectively. This was performed both for temperature melting and salt concentration melting.

This work demonstrated the feasibility of using a lab-on-a-chip magnetoresistive sensor arrays for the characterization of the stability of DNA hybrids as function of both salt concentration and temperature. On a larger sensor array, this

can be used for simultaneous mapping of a number of probe-target interactions in the temperature-salt concentration plane for real-time detection or to identify regions of optimal assay conditions.

Acknowledgements

G.R. acknowledges support from the Danish Council for Independent Research (Postdoc project, DFF-4005-00116).

Notes and references

1 C. Schildkraut and S. Lifson, *Biopolymers*, 1965, **3**, 195–208.
2 K. Knez, D. Spasic, K. P. F. Janssen and J. Lammertyn, *Analyst*, 2014, **139**, 353–370.
3 A. Loy and L. Bodrossy, *Clin. Chim. Acta*, 2006, **363**, 106–119.
4 M. Dufva, J. Petersen and L. Poulsen, *Anal. Bioanal. Chem.*, 2009, **395**, 669–677.
5 L. Strömqvist Meuzelaar, K. Hopkins, E. Liebana and A. J. Brookes, *J. Mol. Diagn.*, 2007, **9**, 30–41.
6 Y. Marcy, P.-Y. Cousin, M. Rattier, G. Cerovic, G. Escalier, G. Béna, M. Guéron, L. McDonagh, F. le Boulaire, H. Bénisty, C. Weisbuch and J.-C. Avarre, *Biotechniques*, 2008, **44**, 913–920.
7 J. Petersen, L. Poulsen, S. Petronis, H. Birgens and M. Dufva, *Nucleic Acids Res.*, 2008, **36**, e10.
8 A.-E. Surkus and G.-U. Flechsig, *Electroanalysis*, 2009, **21**, 1119–1123.
9 A. H. J. Yang, K. Hsieh, A. S. Patterson, B. S. Ferguson, M. Eisenstein, K. W. Plaxco and H. T. Soh, *Angew. Chemie*, 2014, **126**, 3227–3231.
10 R. Meunier-Prest, S. Raveau, E. Finot, G. Legay, M. Cherkaoui-Malki and N. Latruffe, *Nucleic Acids Res.*, 2003, **31**, e150.
11 J. B. Fiche, a Buhot, R. Calemczuk and T. Livache, *Biophys. J.*, 2007, **92**, 935–946.
12 C. E. Wagner, L. J. A. Macedo and A. Opdahl, *Anal. Chem.*, 2015, **87**, 7825–7832.
13 S. Mahajan, J. Richardson, T. Brown and P. N. Bartlett, *J. Am. Chem. Soc.*, 2008, **130**, 15589–15601.
14 G. Rizzi, F. W. Østerberg, A. D. Henriksen, M. Dufva and M. F. Hansen, *J. Magn. Magn. Mater.*, 2015, **380**, 215–220.
15 J. Petersen, L. Poulsen, H. Birgens and M. Dufva, *PLoS One*, 2009, **4**, e4808.
16 G. Lin, D. Makarov and O. G. Schmidt, *Lab Chip*, 2017.
17 D. Issadore, Y. I. Park, H. Shao, C. Min, K. Lee, M. Liong, R. Weissleder and H. Lee, *Lab Chip*, 2014, **14**, 2385–2397.
18 G. Rizzi, J.-R. Lee, P. Guldberg, M. Dufva, S. X. Wang and M. F. Hansen, *Biosens. Bioelectron.*, 2017, **93**, 155–160.
19 G. Rizzi, F. W. Østerberg, M. Dufva and M. Fougt Hansen, *Biosens. Bioelectron.*, 2014, **52**, 445–451.
20 R. S. Gaster, L. Xu, S.-J. Han, R. J. Wilson, D. a Hall, S. J. Osterfeld, H. Yu and S. X. Wang, *Nat. Nanotechnol.*, 2011, **6**, 314–20.
21 F. W. Østerberg, B. T. Dalslet, D. Snakenborg, C. Johansson, M. F. Hansen, U. Häfeli, W. Schütt and M. Zborowski, AIP Publishing, 2010, vol. 1311, pp. 176–183.
22 A. L. Koh and R. Sinclair, in *Technical Proceedings of the 2007 NSTI Nanotechnology Conference and Trade Show*, NSTI, 2007, pp. 101–104.